Figure captions and figures

Figure 1 (a) Location of Lake Kinneret (star) in the Eastern Mediterranean Region; (b) Jordan Rift Valley (satellite images for (a) and (b) are from Imagery©2016 TerraMetrics); (c) Lake Kinneret with location of two 2010 coring sites Ki I and Ki II. Bathymetry given in 5 m intervals (after Berman et al., 2014, background after NASA). The major in- and outflow of the lake is the Jordan River. Further inflows starting clockwise from the city of Tiberias are: Rakat, Amud, Korazim, Koach, Meshushim, Yehudia, Bitra, Dalyot, Sfamnum, Kanaf, Samach, Ein Gev, and Yavneel (Berman et al., 2014). (d) Average monthly rainfall and average temperatures (daily maxima and minima) for the city of Tiberias (time-series from 1976-1995, www.worldweather.org).

Figure 2: Age-to-depth model of the Lake Kinneret composite profile based on calibrated radiocarbon data. Error bars indicate 2 σ-range. Black arrows display reservoir correction at depth horizons (358 cm, 794 cm, and 944 cm) with available macro and bulk organic samples. DAZ1-4 correspond to defined diatom assemblage zones (modified after Schiebel and Litt, 2017)

Figure 3 Summary diatom diagram from Lake Kinneret (composite profile from core KI_10_I and KI_10_II) showing selected taxa (present at > 5 % abundance), diatom concentration and Plankton/Benthos (P/B)-ratio. Some of the rare benthic taxa are grouped together at genus level (e.g. *Amphora* spp., *Achnanthes* spp., *Nitzschia* spp., *Navicula* spp.). Diatom assemblage zones (DAZ) are defined by CONISS cluster analysis. The calibrated radiocarbon chronology (Schiebel and Litt, 2017) is marked at 500-year intervals, with an estimated age of 9,000 cal yrs BP at the base of the sequence. In the marked sections of the diagram (grey pattern) diatoms were rare (17.8-16.9 m; 15.4-14.8 m depth) or not well preserved and absent in one sample (4.57 m depth). **Figure 4** The presented *clr*-biplot for the geochemical data of Lake Kinneret segregates the individual diatom zones (DAZs; different coloured dots). The length of the link (blue bar) between Fe and Ti, shows that the variance between the pair of elements [Fe, Ti] is smaller than the variance between the pair [Fe, Si], for instance. When the variance value in between elements is relative small, they are correlated to each other, and their respective rays (red vectors) tend to point to similar directions. The elements [Ca, Sr] show relative small variance representing the carbonate accumulation. The elements [Fe, Ti, K, Si] also show relative small variance, representing the detrital fraction.

Figure 5 Multi-proxy data from Lake Kinneret (composite profile from core KI_10_I and KI_10_II) showing a selected dataset of diatoms, geochemistry, mineralogy and palynology plotted against age [cal yrs BP] and depth [cm]. Pollen data was provided by Schiebel (2013): "typical steppe vegetation" here includes all species of the following families: *Apiaceae*, *Asteraceae*, *Chenopodiaceae*, *Poaceae* and *Polygonum*. A detailed pollen analysis is published in Schiebel and Litt (2017).

Figure 6 Comparison of currently known, fragmentary Holocene lake-level reconstructions from the Dead Sea (Kushnir and Stein, 2010) and Lake Kinneret (Hazan et al., 2005) compared to the reconstructed lake-level curve inferred from shifts in the ratio of planktonic to benthic (P/B) diatom taxa (grey curve shows P/B-ratio for diatoms in high resolution; black curve is a 10 point average for the P/B-ratio). The presented lake-level reconstruction for the Dead Sea is a combination of absolute lake-level curves (based on the identification of palaeo-shorelines and knowledge of their age and original elevation) and relative lake-level curves (based on estimates of relative water depth identified by lithological changes in sediment cores) and were

compiled for the Holocene by Kushnir and Stein (2010). The presented lake-level reconstruction for Lake Kinneret by Hazan et al. (2005) is based on sedimentological identification of radiocarbon-dated palaeo-shorelines. Note that some intervals of the curves are dashed and labelled with question marks, indicating that they are assumptions and not robust curve reconstructions. Assumed correlations between the Dead Sea and Lake Kinneret curves are marked for a better comparison.

Figure 7 A putative event layer in core Ki_I_4.3-5.3 showing inverse grading and contrasting lithology compared to the rest of the record, correlating with marked shifts in geochemical and mineralogical indicators. Each star represents one sample. The light grey line denotes a sample containing no diatoms.

Figure 1

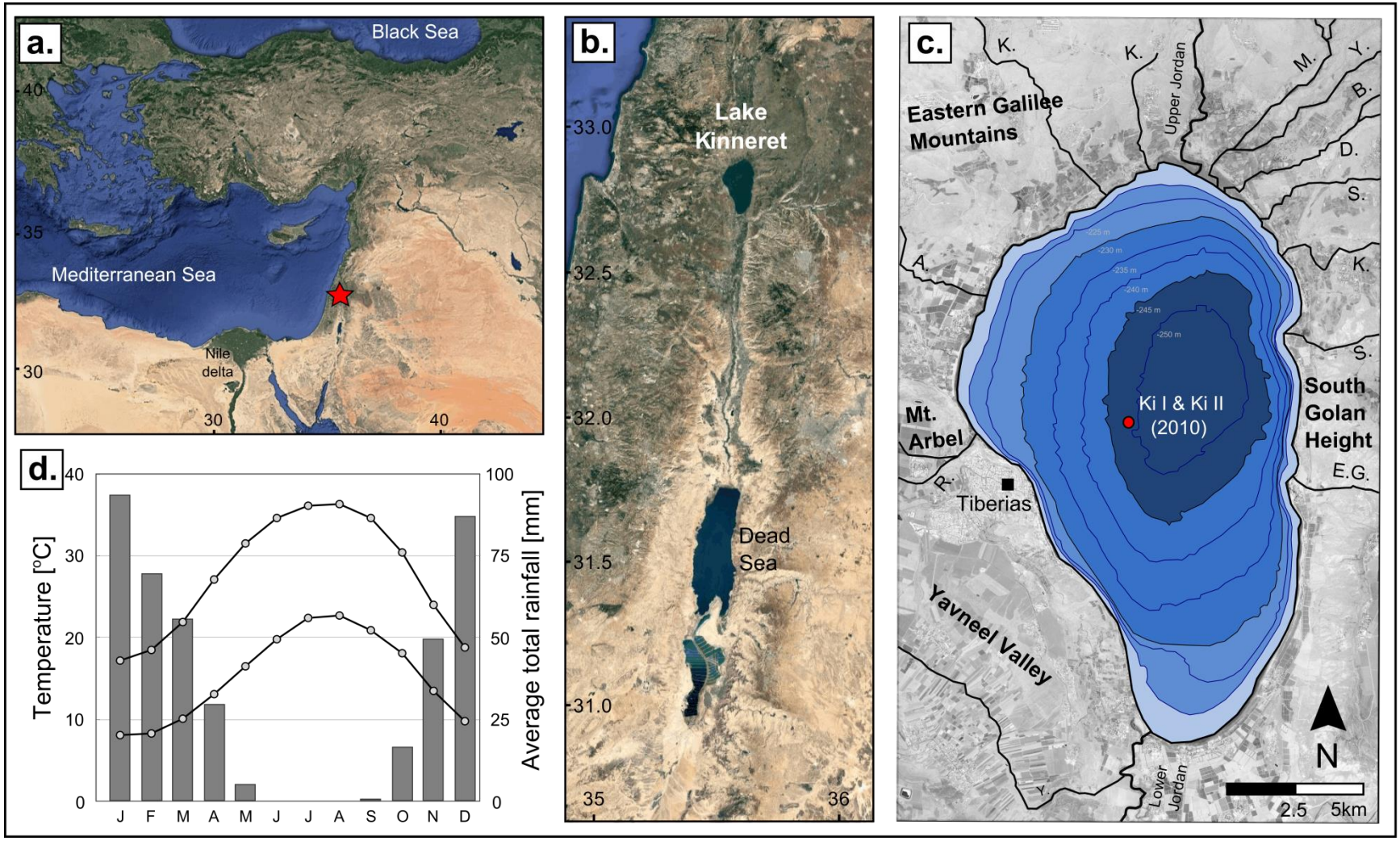
a.
Black Sea
Mediterranean Sea
Nile
delta
40
35
30
30
40
b.
Lake
Kinneret
Dead
Sea
33.0
32.5
32.0
31.5
31.0
35
36
c.
Eastern Galilee
Mountains
Upper Jordan
Mt.
Arbel
Tiberias
Ki I & Ki II
(2010)
South
Golan
Height
E.G.
Yavneel Valley
Lower
Jordan
N
2.5
5km
d.
Temperature [°C]
Average total rainfall [mm]
J F M A M J J A S O N D

Figure 2

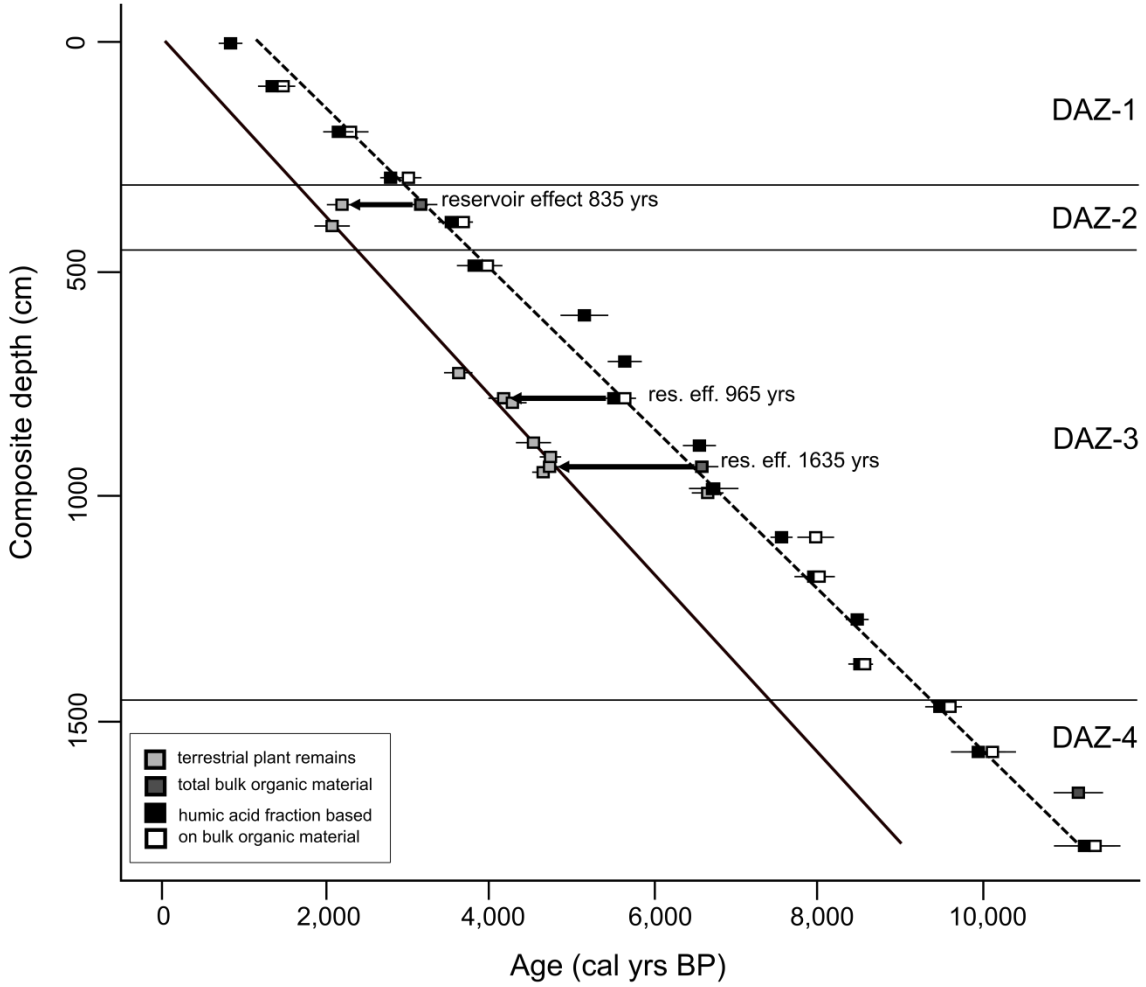
Composite depth (cm)
0
500
1000
1500
DAZ-1
DAZ-2
DAZ-3
DAZ-4
reservoir effect 835 yrs
res. eff. 965 yrs
res. eff. 1635 yrs
terrestrial plant remains
total bulk organic material
humic acid fraction based
on bulk organic material
0
2,000
4,000
6,000
8,000
10,000
Age (cal yrs BP)

Figure 3

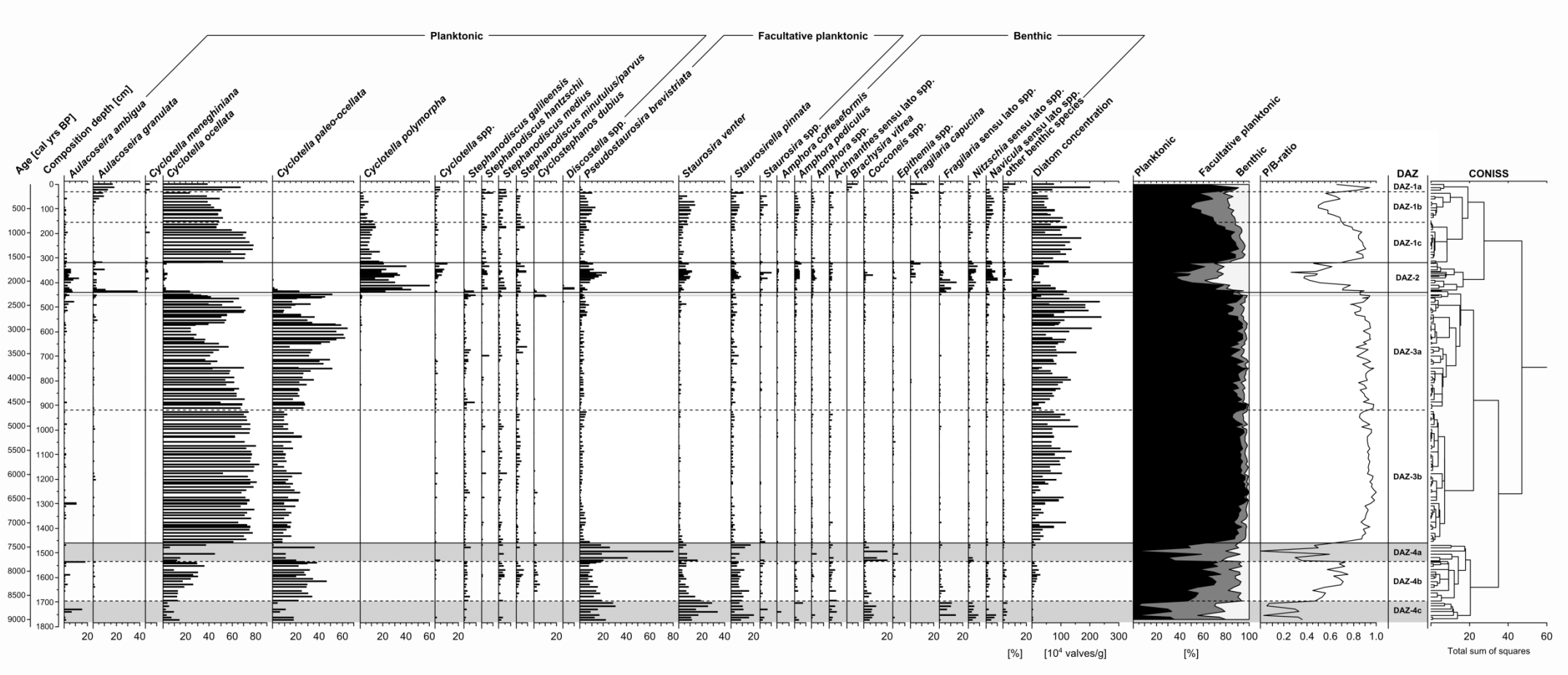
Planktonic
Facultative planktonic
Benthic
Age [cal yrs BP]
Composition depth [cm]
Aulacoseira ambigua
Aulacoseira granulata
Cyclotella meneghiniana
Cyclotella ocellata
Cyclotella paleo-ocellata
Cyclotella polymorpha
Cyclotella spp.
Stephanodiscus galileensis
Stephanodiscus hantzschii
Stephanodiscus medius
Stephanodiscus minutulus/parvus
Cyclostephanos dubius
Discostella spp.
Pseudostaurosira brevistriata
Staurosira venter
Staurosirella pinnata
Staurosira spp.
Amphora coffeaeformis
Amphora pediculus
Amphora spp.
Achnanthes sensu lato spp.
Brachysira vitrea
Cocconeis spp.
Epithemia spp.
Fragilaria capucina
Fragilaria sensu lato spp.
Nitzschia sensu lato spp.
Navicula sensu lato spp.
other benthic species
Diatom concentration
Planktonic
Facultative planktonic
Benthic
P/B-ratio
DAZ
CONISS
DAZ-1a
DAZ-1b
DAZ-1c
DAZ-2
DAZ-3a
DAZ-3b
DAZ-4a
DAZ-4b
DAZ-4c
[%]
[10^4 valves/g]
[%]
Total sum of squares

Figure 4

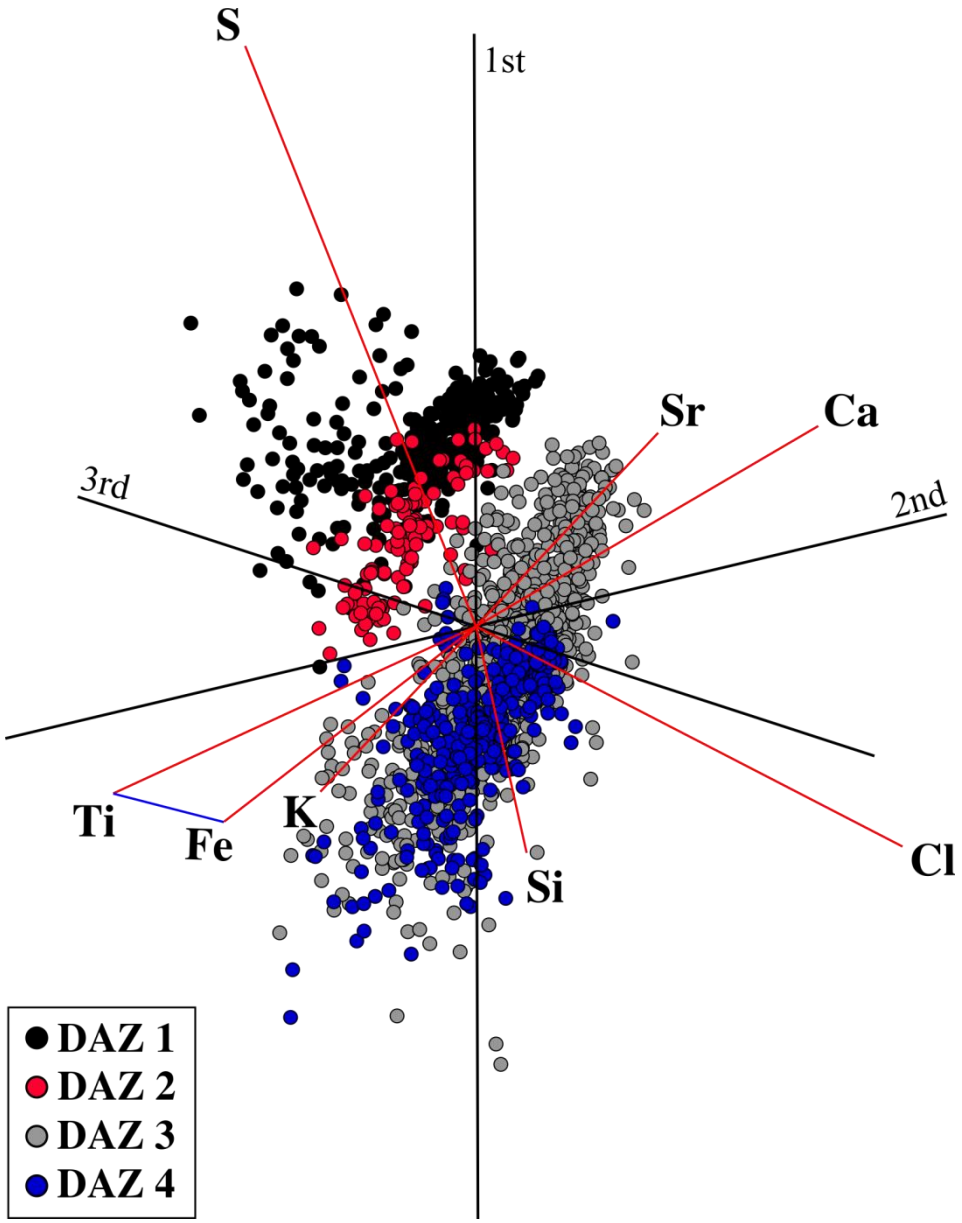

Figure 5

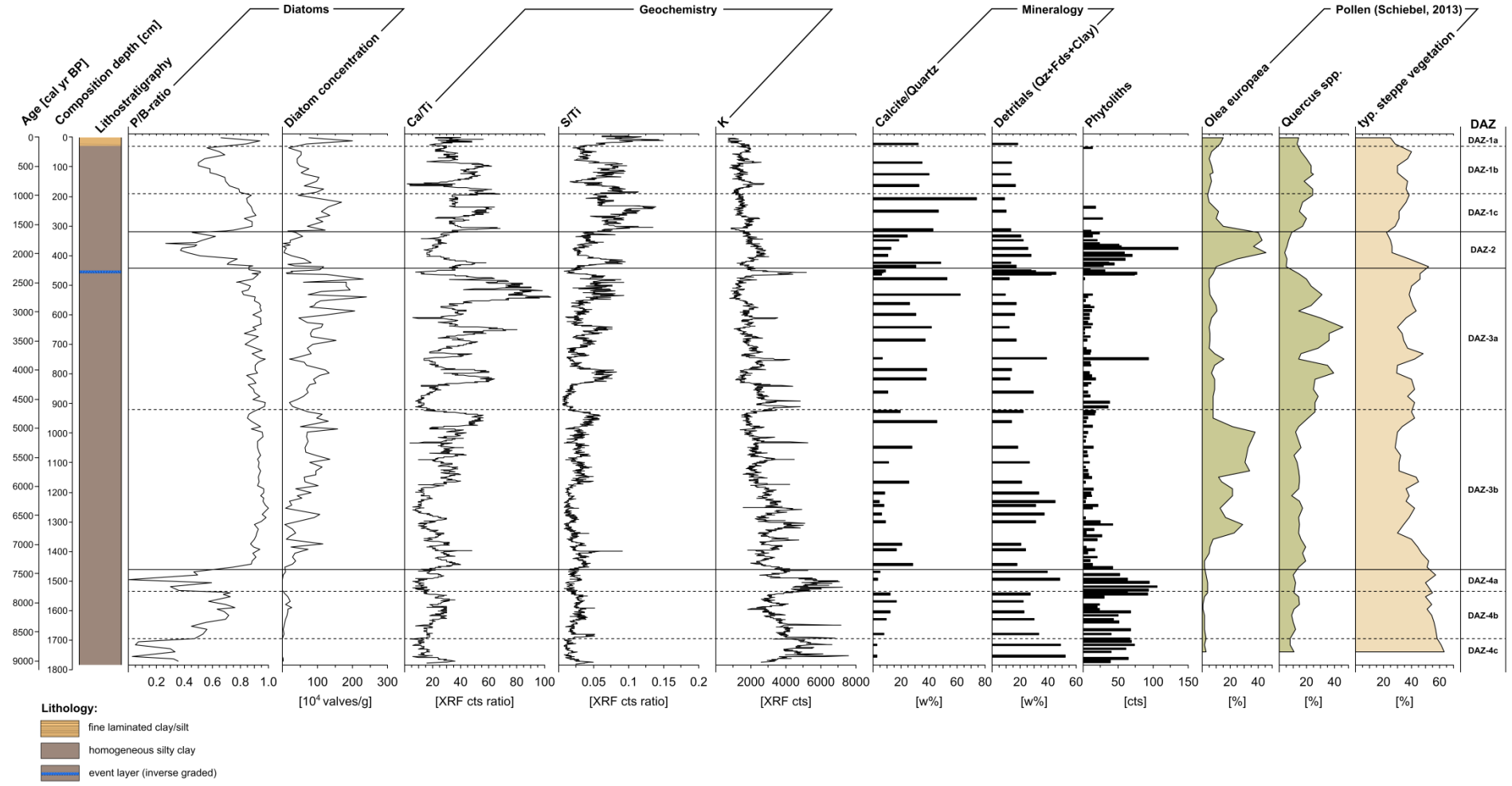
Diatoms
Geochemistry
Mineralogy
Pollen (Schiebel, 2013)
Age [cal yr BP]
Composition depth [cm]
Lithostratigraphy
P/B-ratio
Diatom concentration
Ca/Ti
S/Ti
K
Calcite/Quartz
Detritals (Qz+Fds+Clay)
Phytoliths
Olea europaea
Quercus spp.
typ. steppe vegetation
DAZ
DAZ-1a
DAZ-1b
DAZ-1c
DAZ-2
DAZ-3a
DAZ-3b
DAZ-4a
DAZ-4b
DAZ-4c
[10⁴ valves/g]
[XRF cts ratio]
[XRF cts ratio]
[XRF cts]
[w%]
[w%]
[cts]
[%]
[%]
[%]
Lithology:
fine laminated clay/silt
homogeneous silty clay
event layer (inverse graded)

Figure 6

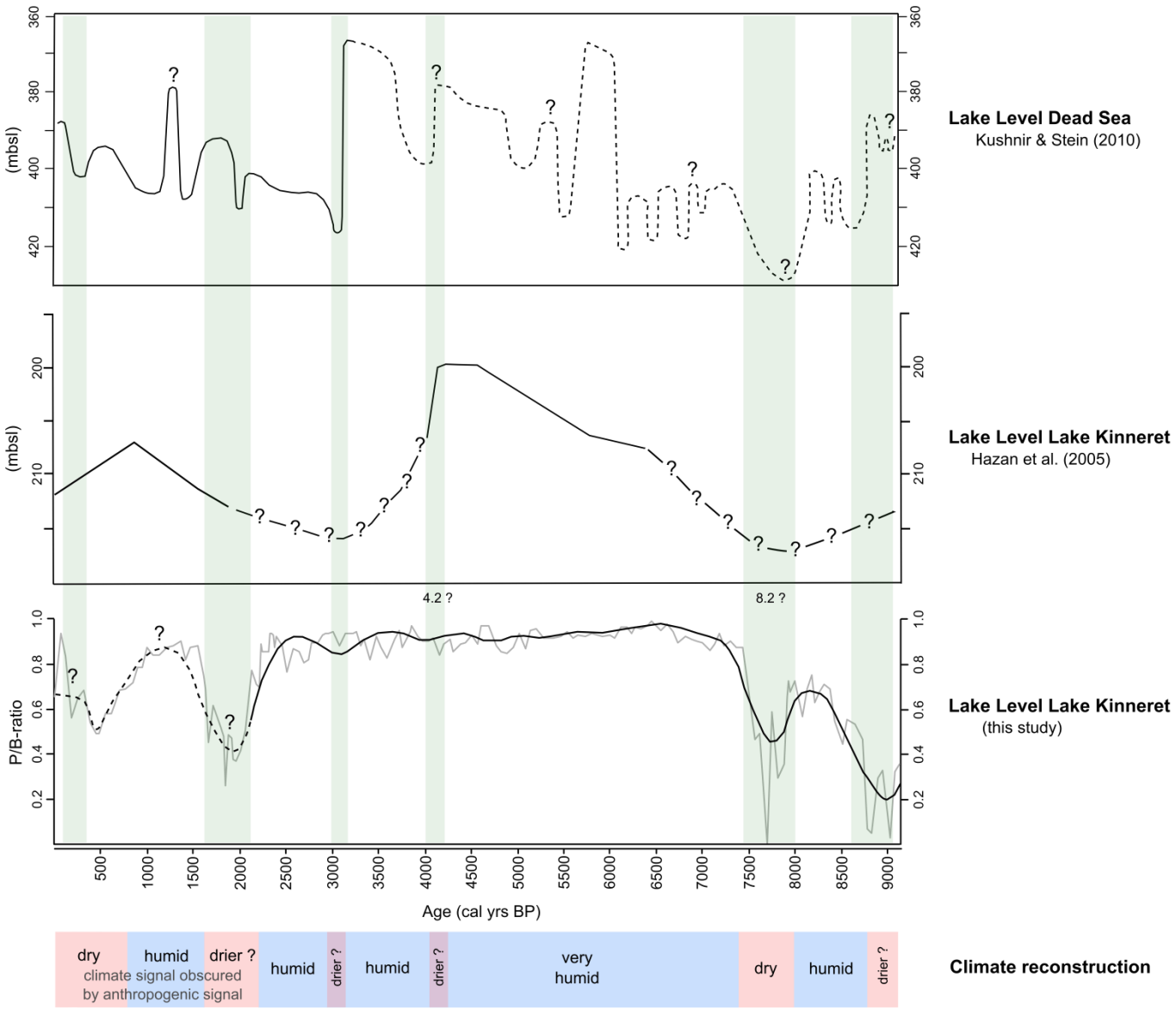
(mbsl)
360
380
400
420
Lake Level Dead Sea
Kushnir & Stein (2010)
(mbsl)
200
210
Lake Level Lake Kinneret
Hazan et al. (2005)
4.2 ?
8.2 ?
P/B-ratio
0.2
0.4
0.6
0.8
1.0
Lake Level Lake Kinneret
(this study)
500
1000
1500
2000
2500
3000
3500
4000
4500
5000
5500
6000
6500
7000
7500
8000
8500
9000
Age (cal yrs BP)
dry
climate signal obscured
by anthropogenic signal
humid
drier ?
humid
drier ?
humid
drier ?
very
humid
dry
humid
drier ?
Climate reconstruction

Figure 7

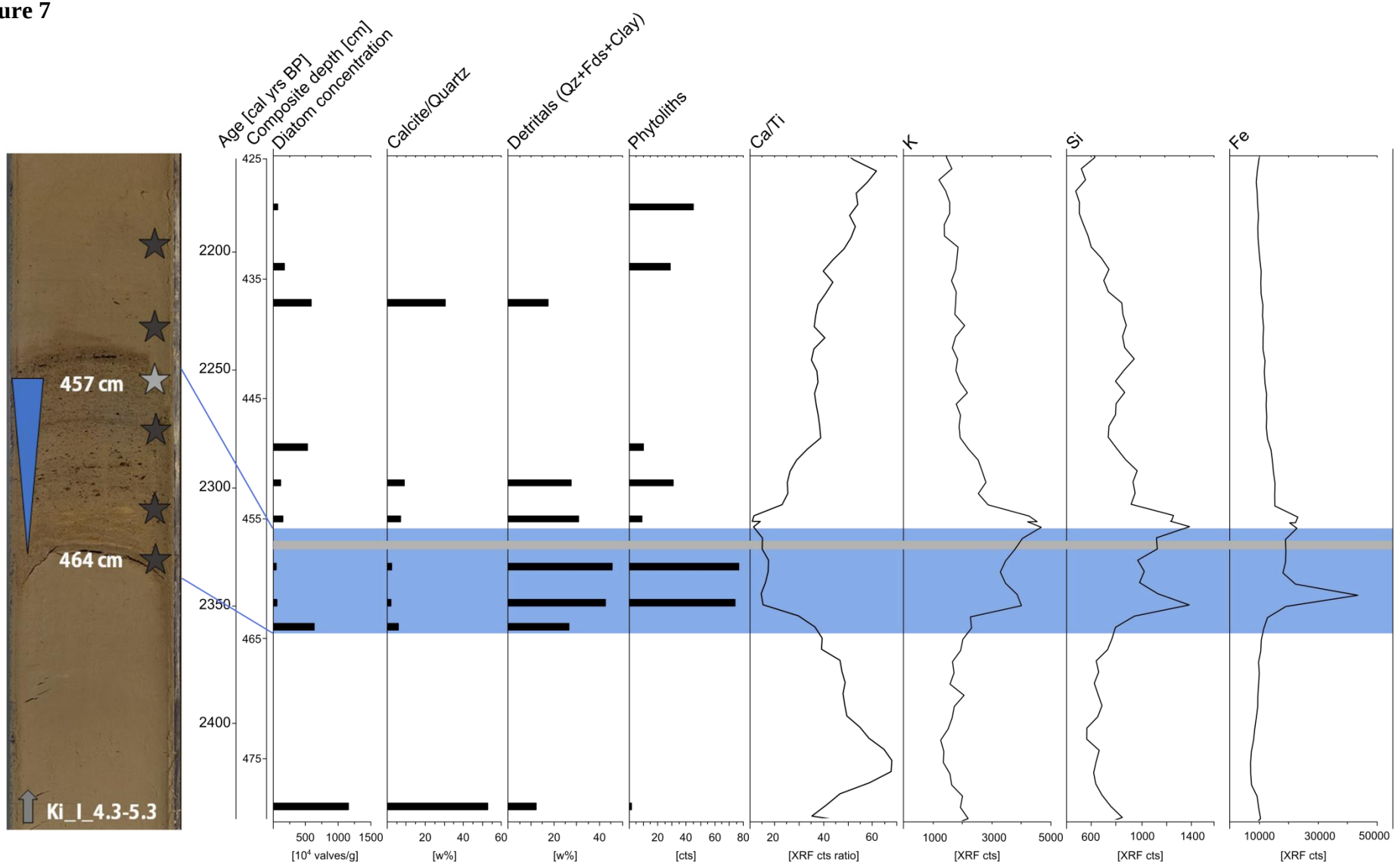
Age [cal yrs BP]
Composite depth [cm]
Diatom concentration
Calcite/Quartz
Detritals (Qz+Fds+Clay)
Phytoliths
Ca/Ti
K
Si
Fe
457 cm
464 cm
Ki_I_4.3-5.3
2200
2250
2300
2350
2400
425
435
445
455
465
475
500 1000 1500
[10⁴ valves/g]
20 40 60
[w%]
20 40
[w%]
20 40 60 80
[cts]
20 40 60
[XRF cts ratio]
1000 3000 5000
[XRF cts]
600 1000 1400
[XRF cts]
10000 30000 50000
[XRF cts]